JOURNAL OF GEOPHYSICAL RESEARCH, VOL. 101, NO. C7, PAGES 16,601–16,613, JULY 15, 1996

Directional spreading function of the sea wave spectrum at short scale, inferred from multifrequency radar observations

G. Caudal and D. Hauser

Centre d'Étude des Environnements Terrestre et Planétaires, Vélizy, France

Abstract. Several models of the directional spreading function of the sea wave spectrum have been proposed in the literature for low wavenumbers. In this paper we propose a high-wavenumber extrapolation of those models, obtained by fitting a correcting term which vanishes at large scales (low wavenumbers). At short scales (high wavenumbers) the correcting term is constrained by multifrequency microwave observations of the normalized radar cross section σ° from *P* band (frequency = 0.43 GHz) up to *Ka* band (frequency = 34.43 GHz), together with optical observations of the sea surface slope variance. Two formulations are given, one providing a high-wavenumber extrapolation to *Apel*'s [1994] formulation and the other providing a high-wavenumber extrapolation to *Donelan et al.*'s [1985] and *Banner*'s [1990] formulation. The correcting term δ, expressed as a function of wavenumber k and wind speed U by means of six least squares fitted parameters, is found to vary strongly with k and slightly with U. Another simpler expression for δ, involving only the dependence with k by means of three fitted parameters, is therefore also proposed. According to our fitted model of the spreading function, there is a spectral region in the short gravity range where the sea spectrum shows only a weak dependence on the direction, in accordance with the previous models. However, unlike them, our model gives an increase of the anisotropy of the spreading function at higher wavenumbers, in such a way that the ratio between the cross-wind and along-wind spectral densities of the folded spectrum is reduced to no more than 35% at high wavenumbers ($k \approx 1000$ rad/m). This increase of anisotropy at high frequency is in accordance with conclusions drawn by previous authors from radar backscatter data, which were, however, limited to narrow spectral bands since their analyses involved only single-frequency radar data.

1. Introduction

The azimuthal behavior of the two-dimensional spectrum of the sea waves may be observed in the field by means of different in situ and remote sensing techniques according to the domain of wavenumber studied. Observations of the directional wave spectra made during the Joint North Sea Wave Project (JONSWAP) 1973 [*Hasselmann et al.*, 1980], as well as observations by *Donelan et al.* [1985], concerned wavenumbers up to ≈10 times the spectral peak. The JONSWAP directional wave spectra were obtained from pitch-and-roll and meteorological buoys, while *Donelan et al.*'s [1985] observations were performed by means of an array of capacitive wave staffs suspended from a research tower in Lake Ontario. *Banner et al.* [1989] measured the short gravity waves by means of stereophotogrammetry from an oil platform under open ocean conditions. Those observations have led *Banner* [1990] to propose a spectral model in which the wave spectral directionality varies from narrow near spectral peak to broad in the short gravity range. *Apel* [1994] extended such kind of formulation up to the gravity capillary domain. On the other hand, models based upon observations of radar backscatter tend to propose narrow directional spreading at short scale [*Fung and Lee*, 1982; *Durden and Vesecky*, 1985; *Caudal and Le Proud'hom*, 1994]. Each of those radar-inferred models, however, was based on a limited set of data involving only one radar frequency. For incidence angles greater than ≈25° the radar cross section of the sea surface is principally sensitive to the spectral density of the sea waves at the Bragg resonant wavenumber, which is of the same order of magnitude as the electromagnetic wavenumber. Therefore those radar observations were unable to document a large domain of wavenumbers of the wave spectrum.

Paper number 96JC00921.
0148-0227/96/96JC-00921$09.00

The purpose of this paper is to perform a more systematic use of available observations of the radar cross section obtained at different radar frequencies, in order to be able to study the behavior of the anisotropy at short scale over the widest spectral range possible. The directional wave spectra reported by *Hasselmann et al.* [1980], *Donelan et al.* [1985], or *Banner et al.* [1989] did not involve sea waves with lengths shorter than 20 cm, and therefore the radar should be useful to constrain the models at shorter scales. The idea here is therefore to propose a correcting term to the spreading function proposed by *Banner* [1990] or *Apel* [1994]. This correcting term should leave those models almost unmodified at large scale (from spectral peak to wavelengths of the order of 20 cm, where those models are constrained by the observations) but should conform to the radar observations at shorter scales.

In order to produce an observationally constrained model, a formulation of a wave spectral model will be chosen, in which the spreading function will include a correcting term with tunable parameters. The tuning of those parameters will be performed through comparison to a set of observed backscatter data obtained at various radar frequencies, polarization states, incidence angles, and wind conditions. The link between the sea surface spectral description and radar backscatter data will be obtained through an electromagnetic model. The set of parameters will be determined through a least squares procedure. The description of the sea spectral model and electromagnetic model, together with the fitting procedure, will be given in section 2. The set of data used as input will be described in section 3, and the results of the fit will be presented in section 4.

2. Methodology

As discussed above the principle of our method consists of tuning a wave spectral model in order to fit the observations through an electromagnetic model. Therefore we shall first describe the wave spectral model and the electromagnetic model, before describing the tuning technique itself.

2.1. Wave Spectral Model

2.1.1. Directional wave spectrum. Increasingly more sophisticated models of the directional wave spectrum of the sea have been proposed as the quantity and quality of available data increased. In most cases the directional wave spectrum is described as a function $F(k, \varphi)$ of wavenumber k and azimuth φ (with $\varphi = 0$ taken along the wind direction) as follows:

$$F(k, \varphi) = F(k, 0)D(k, \varphi) \tag{1}$$

where $D(k, \varphi)$ is the directional spreading function (with $D(k, 0) \equiv 1$). We shall assume that the wind is sufficiently steady that the dominant wind waves are directed along the wind direction ($\varphi = 0$). The work by *Donelan et al.* [1985] and *Banner* [1990] has led to the following expression for $D(k, \varphi)$ valid both near the peak region and in the equilibrium range:

$$D(k, \varphi) = \operatorname{sech}^2 \beta\varphi \tag{2}$$

where β is given as

$$\beta = \beta_o = 2.28(k/k_p)^{-0.65} \qquad 0.97 < k/k_p < 2.56 \tag{3a}$$

$$\beta = \beta_o = 10^{-0.4+0.839 \exp[-0.567 \ln(k/k_p)]} \qquad k/k_p > 2.56 \tag{3b}$$

in which k_p is the wavenumber of the spectral peak. In this paper we shall consider fully developed waves only, and in that condition, k_p is given by *Donelan and Pierson* [1987] in terms of the acceleration of gravity g and the 10-m wind velocity U as

$$k_p = \frac{g}{(1.2U)^2} \tag{4}$$

Apel [1994] proposed the following alternative expression for $D(k, \varphi)$, matching the Donelan-Banner spreading function to within the experimental errors:

$$D(k, \varphi) = \exp(-\alpha\varphi^2) \tag{5a}$$

with

$$\alpha = \alpha_o = 0.14 + 5.0(k/k_p)^{-1.3} \tag{5b}$$

Apel's work was performed from a compilation of recent work done by several investigators [*Donelan et al.*, 1985; *Donelan and Pierson*, 1987; *Banner*, 1990; *Jahne and Riemer*, 1990], and his model is given for wavenumbers up to 1500 rad/m (i.e., wavelength ≈ 0.4 cm). The description of the spectral density in the wind direction $F(k, 0)$ proposed by Apel will therefore be used unchanged in this paper (see Appendix A). We argue, however, that the description of the spreading function $D(k, \varphi)$ initially proposed by *Banner* [1990] for the equilibrium range only, and given either by our equations (2), (3a), and (3b) or (5a)–(5b), cannot be extrapolated beyond the equilibrium range to the gravity capillary domain. Starting, for example, from (5a)–(5b), we therefore include a correction, leading to the following expression replacing (5b):

$$\alpha = 0.14 + 5.0(k/k_p)^{-1.3} + \delta \tag{5c}$$

The additional term δ (equal to zero in Apel's model) is a function of wavenumber and possibly also of wind velocity. It should become significant only at high k. It will be formally expressed as a parameterized function

$$\delta = \delta(k, U, p_1, p_2, \ldots, p_m) \tag{6}$$

where $p_1, p_2, \ldots, p_m$ are adjustable parameters.

2.1.2. Folded wave spectrum. Most electromagnetic models relate the radar cross section of the sea to the spectral properties of the sea surface (see section 2.2 below). However, the spectrum concerned by electromagnetic models is not the directional wave spectrum $F(k, \varphi)$ but rather the ordinary two-dimensional spectrum $F_s(k, \varphi)$, which is the Fourier transform of the covariance function of a frozen spatial image of the sea surface. As such it has a reflectional symmetry in wavenumber:

$$F_s(k, \varphi) = F_s(k, \varphi + \pi) \tag{7}$$

$F_s(k, \varphi)$ therefore provides no information about the direction of propagation of the Fourier components. It can be deduced from the directional wave spectrum through

$$F_s(k, \varphi) = 0.5[F(k, \varphi) + F(k, \varphi + \pi)] \tag{8}$$

The azimuthal behavior of $F_s(k, \varphi)$ can be similarly described by means of a folded spreading function $D_s(k, \varphi)$:

$$D_s(k, \varphi) = 0.5[D(k, \varphi) + D(k, \varphi + \pi)] \tag{9}$$

This point has been discussed in detail by *Banner* [1990]. Examples of the polar plots of $D(k, \varphi)$ and $D_s(k, \varphi)$ are given in Figure 1.

This work is based upon radar or optical observations and is therefore unable to document $D(k, \varphi)$ directly. It can only give indirect information through $D_s(k, \varphi)$, provided that a suitable model for the functional form of $D(k, \varphi)$ is chosen. In this paper we make the assumption that the functional form of the directional spreading function $D(k, \varphi)$ given at low wavenumbers (equations (2) or (5a)) can be extrapolated toward high wavenumbers. Let us for instance take the Donelan-Banner formulation (equation (2)). Our approach is based upon the following principle: For given β we determine $D(k, \varphi)$ from (2) and then $D_s(k, \varphi)$ from (9), and finally, we perform the comparison between $D_s(k, \varphi)$ and the data, in order to find the value of β which optimizes the fit between model and data, within the assumption that (2) holds.

2.2. Electromagnetic Model

In order to compute the normalized radar cross section σ^o of the surface from the wavenumber spectrum described above, we use basically the same electromagnetic model as *Donelan and Pierson* [1987]. That model is given in Appendix B. To summarize, the electromagnetic model consists of the two-scale (tilted plane) model [*Valenzuela*, 1978; *Ulaby et al.*, 1982] which accounts for the Bragg component of the backscatter (which dominates at high incidence angles), to which one adds the specular (geometric optics) component (which dominates at low incidence). *Ulaby et al.* [1982] reported that such a combined model does not produce good agreement with the backscattering measurements within 25° of the vertical but that at large angles of incidence the agreement is satisfactory. Obviously, the domain of the transition between Bragg dominated backscatter and specular backscatter is somewhat tricky. Since at very high incidence angles (say, $\theta > 65°$) another difficulty arises when shadowing becomes nonnegligible, we chose to limit the range of incidence probed to $30° \leq \theta \leq 60°$.

2.3. Model/Data Comparison and Inversion Technique

Once the functional form for the spreading function has been chosen (equation (6)), the aim of our study is to determine the set of parameters $p_1, p_2, \cdots, p_m$ which leads to the best fit between model and observations. The combination of the wave spectral model and the electromagnetic model gives the function $\sigma°(\theta, \varphi, f, U, pp)$ as soon as the set of parameters $\{p_1, p_2, \cdots, p_m\}$ has been given (here θ is incidence, φ is azimuth, U is wind velocity, f is radar frequency, and pp is polarization). This function has to be compared to observations.

Since the aim of our study is to document the spreading function, our observations should give information on the ratio between the along-wind and cross-wind normalized radar cross sections (NRCS) ($\sigma°_{al}$ and $\sigma°_{cr}$, respectively). Note that the standard two-scale electromagnetic model with Gaussian slope probability density function (pdf) (see Appendix B) relates the spectrum of the sea surface to $\sigma°$, excluding any third-order moment of the sea surface statistics and therefore by construction the upwind and downwind NRCSs ($\sigma°_{up}$ and $\sigma°_{do}$) obtained through the electromagnetic model cannot be distinguished from each other. On the other hand, the maxima of $\sigma°(\varphi)$ which are really observed in the upwind and downwind directions usually differ from each other, with $\sigma°_{up} > \sigma°_{do}$ in general. This well-known feature is due to the non-Gaussian nature of the sea surface statistics. It is illustrated in Figure 2 where a typical example of $\sigma°(\varphi)$ obtained from our airborne radar Radar pour l'Etude du Spectre des Surfaces par Analyse Circulaire (RESSAC) (see section 3.6 below) is given. Note, however, that although the amplitudes of both maxima are different, the most prominent feature of the azimuthal signature of $\sigma°$ is the depletion of $\sigma°$ in both cross-wind directions, compared to either $\sigma°_{up}$ or $\sigma°_{do}$. In order to compare the outputs of the electromagnetic model to the observations, we therefore take the observations of $\sigma°_{up}$ and $\sigma°_{do}$, from which we define the "along-wind" NRCS $\sigma°_{al} = (\sigma°_{up} + \sigma°_{do})/2$. We then compute the ratio $r = \sigma°_{al}/\sigma°_{cr}$. This quantity r (expressed in decibels) is the one which we consider as the observed quantity to be used for model inversion.

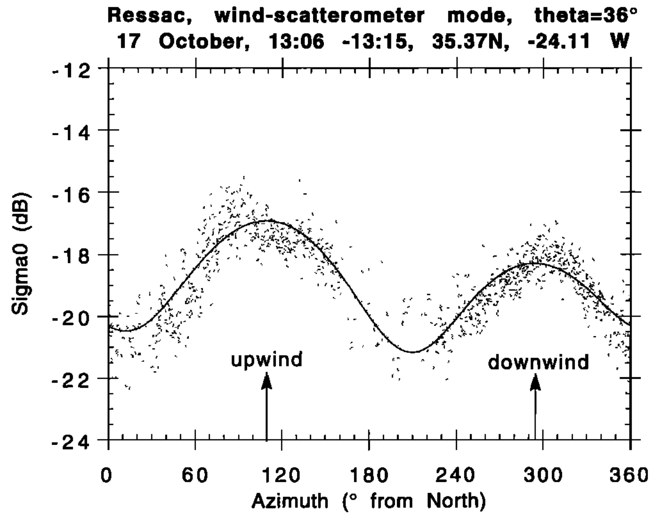

Figure 2. Typical variation of $\sigma°$ versus azimuth angle, obtained with the Radar pour l'Etude de Spectre des Surfaces par Analyse Circulaire (RESSAC) radar during the Semaphore campaign at 36° incidence angle. Three flight circles are combined, yielding a total of about 5000 data points. The solid line is a curve fitted with five coefficients.

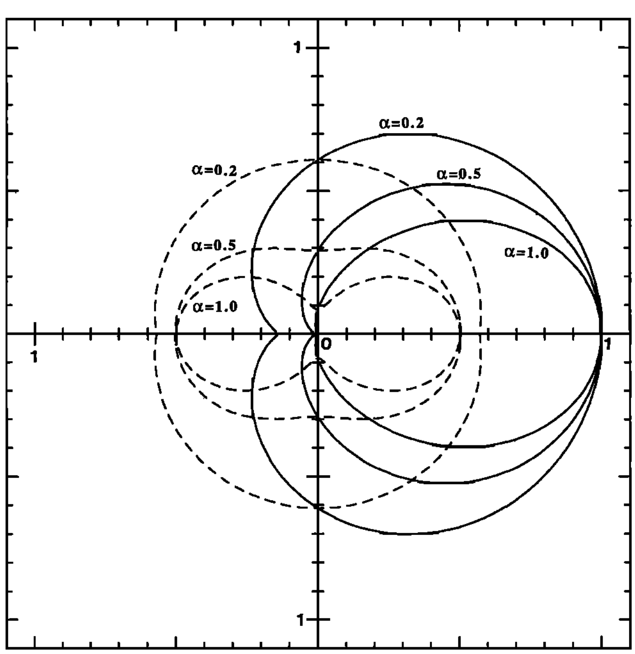

Figure 1. Polar plot of the spreading function given by (5a) for three values of parameter α (α = 0.2, 0.5, and 1.0). Solid lines represent the directional spreading function $D(k, \varphi)$, and dashed lines represent the folded spreading function $D_s(k, \varphi) = 0.5\{D(k, \varphi) + D(k, \varphi + \pi)\}$.

Each data point therefore consists of a value of the ratio r, for a given set of experimental parameters (f, θ, U, pp). We label each data point with a subscript i ($i = 1$ to n). The theoretical values of r for those experimental situations (and for a given set of model parameters $p_1, p_2, \cdots, p_m$) computed by combining the wave spectral model and the electromagnetic model (see above, sections 2.1 and 2.2) may then be written:

$$\begin{aligned} r_1 &= A_1(p_1, p_2, \ldots, p_m) \\ &\vdots \\ r_n &= A_n(p_1, p_2, \ldots, p_m) \end{aligned} \tag{10}$$

If the functions $A_i(p_1, p_2, \cdots, p_m)$ were linear in $p_1, p_2, \cdots, p_m$, we could write the problem as a set of linear equations

$$r_i = \sum_{j=1}^{m} A_{ij} p_j \tag{11}$$

In reality, the functions $A_i(p_j)$ are obviously nonlinear functions of the model parameters. The nonlinearity of the problem will be accommodated by considering it to be locally linear and iterating to the final solution as follows. Assuming that the $A_i(p_j)$ vary smoothly enough, they may be expanded in a Taylor series about a set of initial values of the p_j, say p_j° [e.g., *Jackson*, 1972]:

$$r_i = A_i(p_1^\circ, \ldots, p_m^\circ) + \sum_{j=1}^{m} \left[\frac{\partial A_i}{\partial p_j}\right]_{p_j^\circ} \Delta p_j + \cdots \quad (12)$$

Defining $r_i \equiv A_i(p_1^\circ, \cdots, p_m^\circ) + \Delta r_i$ and ignoring second- and higher-order terms in (12), we have

$$\Delta r_i = \sum_{j=1}^{m} \left[\frac{\partial A_i}{\partial p_j}\right]_{p_j^\circ} \Delta p_j \quad (13)$$

This is the same form as the system of equations (11), with the substitution of Δr_i for r_i, Δp_j for p_j, and

$$[\partial A_i / \partial p_j]_{p_j^\circ} = A_{ij} \quad (14)$$

The system (13) is a set of n linear equations with m unknowns (with $n \gg m$). It is therefore an overconstrained system, which is solved by the standard least squares procedure. The solution $(\Delta p_1, \Delta p_2, \ldots, \Delta p_m)$ gives the displacement vector, or at least the direction along which we must move in the parameter space, leading to the new set of initial values of p_j, say $p_1^1, p_2^1, \ldots, p_m^1$, and the procedure is iterated until convergence is achieved.

3. Observations

3.1. General Comments

As explained above in section 2.2 the domain of incidence angles probed in this study is limited to the range $30° \le \theta \le 60°$, a domain where the Bragg backscattering dominates. In order to document as much of the wave spectrum as possible, the data set that we used was chosen in order to cover the widest range of Bragg wavenumbers as possible. Another objective was to explore how the spectral features identified are varying with wind velocity.

Since we wish to use observations of σ° with various frequencies, those observations necessarily come from an heterogeneous set of data, obtained with various instruments by different experimenters, even though some data sets were obtained with multifrequency radars. Since some scatter occurs from one measurement to the other, most experimenters express their results not in terms of individual measurements, but rather as empirical regression formulas giving σ° as a function of θ, U, φ, f, and pp. The directions examined are usually upwind, downwind, and cross wind, from which the quantity r described in section 2.3 is easily deduced. Most important is the domain of velocities U probed by the authors. Data from aircraft campaigns sometimes probe a limited set of wind situations. In order to be able to define clearly the wind domain within which the results of this study will be applicable, we restrict ourselves to velocities between 3 and 13 m/s, which is a domain of wind speeds well probed by all the data sets that we used. Also, as much as possible, we try to fill a grid which is as regular as possible in terms of velocities and incidence angles. The use of empirical regression formulas built from the observations makes this requirement easier to fill. Thus for all the data sets presented below we take five values of U evenly spaced between 3 and 13 m/s (except for the RESSAC data, as seen in section 3.6 below, for which the highest velocity point at 13 m/s was omitted). Depending upon the authors, the wind velocities are taken at different heights. In this study, all the velocities are rescaled to a height of 10 m. The required corrections are done assuming neutral stability.

As concerns the Bragg wavenumbers, they are necessarily filled in an uneven way, depending on the amount of experiments which have been performed with the various radar frequencies. For example, we identified only one well-documented data set for P band (0.428 GHz, see section 3.3 below), whereas four of our data sets document the C band. We allowed redundancy among those Bragg wavenumbers since data from different sources are independent and combining them will anyhow improve the constraints put on the best fit solution. However, one should avoid having the solution wave spectrum tightly constrained at some wavenumbers and loosely constrained elsewhere by the sole fact that more data were available at some radar frequencies than at others. For this reason an histogram of the various Bragg frequencies was built. This histogram was smoothed, through a mere convolution with a triangular function, and the data points were given a weight which was inversely proportional to the smoothed histogram. The histogram and its smoothed version are given in Figure 3. The different data sources used in this study are described below.

3.2. Multifrequency Data From DUTSCAT

Unal et al. [1991] reported the results of a series of measurements carried out with the airborne Delft University of Technology Scatterometer (DUTSCAT) during the TOSCANE-2 campaign performed over the Atlantic Ocean close to Bretagne (France) in 1987. The system operated at six frequencies (1.2, 3.2, 5.3, 9.65, 13.7, and 17.25 GHz) with both polarizations HH (horizontal) and VV (vertical). The main conclusions are given by *Unal et al.* [1991], while more detailed results are given by *Snoeij et al.* [1992]. The latter authors express the results in terms of an empirical analytic model (6MOD-1 model), in which the NRCS is given as function of wind speed, incidence angle, and azimuth, with the help of a set of 18 tuned coefficients. The authors obtain one set of coefficients for every frequency and polarization. Their 6MOD-1 model, given in their Tables 9-12 and 9-13, has been used here.

To determine the azimuthal behavior of the NRCS, circle flights were performed at three incidence angles, $\theta = 20°$, $30°$, and $45°$. To conform to the domains of θ chosen in section 3.1 ($30° \le \theta \le 60°$), we therefore use only two values for θ ($30°$ and $45°$). The wind velocities which occurred during the flights ranged from $U = 2.5$ m/s to $U = 14$ m/s. Here we take five values of U as described in section 3.1. Because of erroneous data at Ku 2 band (17.25 GHz) with HH polarization and 45°, such a situation is not included in our set of data points. The number of data points that we get here is therefore (6 frequencies $\times$ 2 polarizations $\times$ 2 incidences $\times$ 5 velocities) $-$ (5 erroneous data points) $=$ 115 data points.

3.3. Multifrequency Data From NRL 4-FR and AAFE Radiometer-Scatterometer (RADSCAT)

Jones and Schroeder [1978] compiled the data from several campaigns at various frequencies. Among various studies they explored the behavior of the NRCS anisotropy as a function of

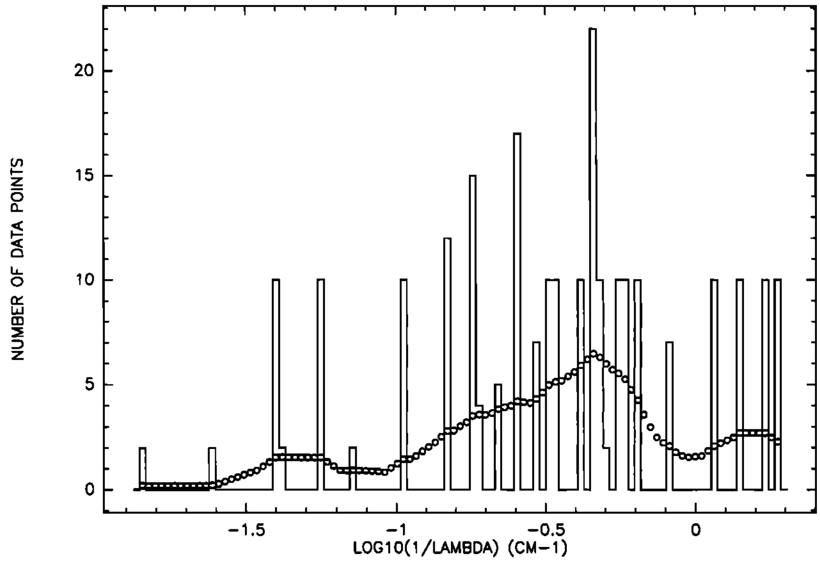

Figure 3. Histogram of the various Bragg frequencies of the data set used. Open circles represent the smoothed histogram.

wind speed or Bragg wavenumber by using the following two sets of data.

The Naval Research Laboratory (NRL) 4-FR data set was obtained with a four-frequency radar (4-FR) by personnel of NRL from 1965 to 1971. The system was an airborne radar operating at X band (8.9 Ghz), C band (4.5 GHz), L band (1.3 GHz), and P band (0.43 GHz). Details of the radar parameters and surface conditions are given by *Daley* [1973]. A wide range of wind conditions occurred, from 0.5 to 47 knots (i.e., 0.3 to 24 m/s). Both polarizations were used.

The AAFE RADSCAT data set was obtained by NASA with an airborne scatterometer operating at 13.9 GHz with both polarizations. As reported by *Jones and Schroeder* [1978], measurements were obtained over open oceans for a variety of surface conditions from light winds and calm seas to gales.

Combining the five frequencies of the data set (four from NRL 4-FR and one from AAFE RADSCAT), *Jones and Schroeder* [1978] performed two kinds of linear regression analyses. The first one consisted of studying the dependence of the upwind/downwind and upwind/cross-wind NRCS ratios upon wind speed. They found that this dependence was weak, and those ratios were found to be either increasing or decreasing with wind speed, according to the frequency, with no apparent trend in frequency. They concluded that the effect of wind speed on those ratios could at first order be ignored.

The second analysis that *Jones and Schroeder* [1978] performed concerned the dependence of those ratios on the Bragg wavelength. In that case they obtained a much more significant effect (see their Figure 7). The NRCS was found to be highly anisotropic for the capillary waves and nearly isotropic for the short gravity waves (approximately 100 cm in length). They fitted the following expression to the measurements:

$$(\sigma^\circ_{\mathrm{up}}/\sigma^\circ_i)_{\mathrm{dB}} = c + z[10\log(1/\Lambda)] \qquad (15)$$

where i = "cr" for crosswind and i = "do" for downwind, $\Lambda = \pi/(k_o \sin\theta)$ is the Bragg wavelength, and c and z are fitted parameters.

Our data points were determined from *Jones and Schroeder*'s [1978] results displayed in their Table 9. Two values of θ (30° and 60°), and the five frequencies with both polarizations were used, thus yielding $2 \times 5 \times 2 = 20$ data points. For comparison to the data the corresponding modeled ratios $r = (\sigma^\circ_{al}/\sigma^\circ_{cr})_{\mathrm{dB}}$ were computed for five values of U evenly spaced between 3 and 13 m/s and then averaged.

3.4. *X* Band and *Ka* Band Data Obtained by the Radio Research Laboratory (RRL)

Masuko et al. [1986] performed dual-polarization NRCS measurements at X band (10.00 GHz) and Ka band (34.43 GHz) in the open sea over two sites off the coasts of Japan in 1980 and 1981, with an airborne scatterometer developed by RRL. Circle flights were performed and data were taken with incidence angles ranging from 0° to 70°. The wind conditions varied between 3.2 and 17.2 m/s. Masuko et al. have compiled their results and expressed the measured NRCS through an empirical expression $\sigma^\circ(U)$ involving two coefficients which themselves depend upon frequency, polarization, incidence angle, and azimuthal direction (upwind, downwind, or cross wind) (see their Table 3). Considering four different incidence angles (30°, 40°, 50°, and 60°), both frequencies and polarizations, and our set of five values of U mentioned above, we then get 80 data points.

3.5. *C* Band ERS 1 Scatterometer Model (VV Polarization)

In conjunction with the launch of the European Space Agency's (ESA) ERS 1 satellite an important effort has been made in Europe to produce empirical models of σ° at C band (5.35 GHz, vertical polarization). In that context a major calibration and validation campaign designated as RENE91 took place in the Norwegian Sea during fall and winter 1991–1992, involving buoys, ship, airplanes, and oil platforms. Those data were used to improve a meteorological wind field model. Both analyzed wind fields and direct buoy measurements were used for model tuning. Among the various versions of the models of σ° which have been proposed, we use here the so-called CMOD2-I3 model described by *Bentamy et al.* [1994], because this recent model also includes data from 16 buoys from the National

Oceanic and Atmospheric Administration (NOAA) network located along the coast of the United States, recorded between March 1992 and April 1993.

The CMOD2-I3 model expresses $\sigma°(\theta, \varphi, U)$ as an analytic expression with 22 coefficients, of which only 12 coefficients concern the along-wind–cross-wind ratio. The model covers essentially the range of wind velocities between 3 and 25 m/s. Due to the geometry of the ERS 1 scatterometer, it is valid for $18° \leq \theta \leq 58°$. We use four evenly spaced values of θ between 30° and 55°, together with our usual set of five values of U (see above), which gives 20 data points.

3.6. *C* Band Data Obtained With RESSAC (HH Polarization)

In order to complement the ERS 1 model described above with horizontal polarization data, we use observations performed by our group with the RESSAC radar. This radar (5.35 GHz, horizontal polarization) has been designed to measure directional spectra of long sea waves (wavelengths $\lambda \geq 50$ m) and operates at low incidence angles ($\theta < 22°$) with a rotating antenna in its standard mode [*Hauser et al.*, 1992]. During the Semaphore campaign in the Azores Islands in 1993 [*Eymard et al.*, 1994] it has also been used in a scatterometer mode, for which the antenna was held fixed with respect to the aircraft and circular flights were performed, allowing it to probe incidence angles between ≈30° and 40°. In situ wind measurements were obtained from buoys and ship [*Eymard et al.*, 1994]. Combining all the data obtained during the campaign, regression formulas were determined directly on the along-wind/cross-wind ratio. Here we have averaged the data from observations around $\theta = 33°$, which is close to the central part of the antenna lobe and thus yields the best accuracy. The linear fit with respect to the 10-m wind speed U gives

$$[\sigma°_{al}/\sigma°_{cr}]_{\mathrm{dB}} = 0.524 + 0.202U(\mathrm{m/s}) \qquad (16)$$

for $\theta = 33°$. Due to the lack of high wind situations during the Semaphore campaign, (16) is given only for the range 2 m/s $\leq U \leq$ 10 m/s. For this reason, from our set of five values of U between 3 and 13 m/s (see section 2.1), we only take the four lowest values here, which yield four data points.

3.7. Optical Observations of Slope Variance

Once the two-dimensional (2-D) wave spectrum $F(k, \varphi)$ has been given, the along-wind and cross-wind slope variances s^2_{al} and s^2_{cr} may be readily obtained through

$$s^2_{al} = \int_0^\infty \int_0^{2\pi} k^2 \cos^2 \varphi F(k, \varphi)\, k dk d\varphi \qquad (17a)$$

$$s^2_{cr} = \int_0^\infty \int_0^{2\pi} k^2 \sin^2 \varphi F(k, \varphi)\, k dk d\varphi \qquad (17b)$$

Because of the factor k^2 in (17a) and (17b) the short scales (wavelengths less than 1 m) play a dominant role in the result of the integration of those equations. One may thus assess the quality of the modeled directional spreading function at short scale by comparing the ratios s^2_{al}/s^2_{cr} inferred from (17a) and (17b) with the measured values. This is the reason why we have added the well-known optical observations by *Cox and Munk* [1954] to our otherwise purely microwave data set. The clean sea empirical model of Cox and Munk gives

$$\frac{s^2_{al}}{s^2_{cr}} = \frac{3.16 \times 10^{-3} U_{12.5}}{0.003 + 1.92 \times 10^{-3} U_{12.5}} \qquad (18)$$

where $U_{12.5}$ is the wind velocity at 12.5-m height and the situations encountered varied from 1 to 14 m/s. In our set of data points the quantity $r' = s^2_{al}/s^2_{cr}$, expressed in decibels, here replaces the quantity r which is used for the radar data (see section 2.3).

Since it integrates all the wavelengths, the constraint on slope variance, unlike radar-inferred constraints, is unable to document the variation of the azimuthal spreading function with k, but it provides a completely independent way to constrain an integral quantity of the spreading function, without the need of any electromagnetic modeling, and is used for this reason. It gives five additional data points corresponding to our usual set of five velocities between 3 and 13 m/s. Since those data points do not correspond to any specific Bragg wavenumber, their weight, as defined in section 3.1 was taken as the mean weight of all the other data points.

4. Results

The different data sets described in the preceding section were merged to provide a total of 244 data points, which served as input to our model inversion process.

4.1. Spreading Function Expressed as exp $(-\alpha\varphi^2)$

In a first attempt the directional spreading function $D(k, \varphi)$ was described by means of (5a) and (5c). In (5c) the additional term δ was written as

$$\delta = \delta_1 = 10^{(p_1U+p_2)X^2+(p_3U+p_4)X+(p_5U+p_6)} \qquad (19)$$

where $X = \log_{10}(k)$ and U and k are expressed in meters per second and radians per meter, respectively.

The iterative process was stopped when the rms error between model and data decreased by less than 10^{-3} dB from one iteration to the next one. The final rms error between model and data is 1.37 dB, and the corresponding set of parameters p_i is

$$\begin{array}{ll} p_1 = -0.0292 & p_4 = 0.0503 \\ p_2 = 0.0636 & p_5 = -0.126 \\ p_3 = 0.127 & p_6 = -0.930 \end{array} \qquad (20)$$

The behavior of coefficient α resulting from (5a) and (5c) with (19) and (20) is displayed in Figure 4, for three values of the wind U. *Apel*'s [1994] unaltered value of α (equation (5b)) is also plotted for comparison (dashed lines). In Figure 4, as well as in the following figures, the lower bound for k is taken as $0.97k_p$, which corresponds to the lower bound considered by *Banner* [1990]. The upper bound is taken as our highest Bragg wavenumber probed, which is 1180 rad/m (i.e., wavelength λ = 0.53 cm). Note that the lowest Bragg wavenumber probed by our data set is k = 9.0 rad/m (i.e., λ = 70 cm).

Our inferred term δ (equation (19)) is therefore constrained only over the wavenumber domain $9 \leq k \leq 1180$ rad/m. It may be argued that for $k < 9$ rad/m, δ is not constrained and may therefore reach completely unrealistic values. It turns out, however, that δ given by (19) and (20) becomes vanishingly small when k is reduced. As can be seen in Figure 4, for every situation considered, δ amounts to less than 35% of the total α in (5c) at k = 9 rad/m and reduces to less than 3% of α at k = 1 rad/m, and this proportion decreases further at lower k. The effect of δ at low wavenumbers is therefore entirely negligible.

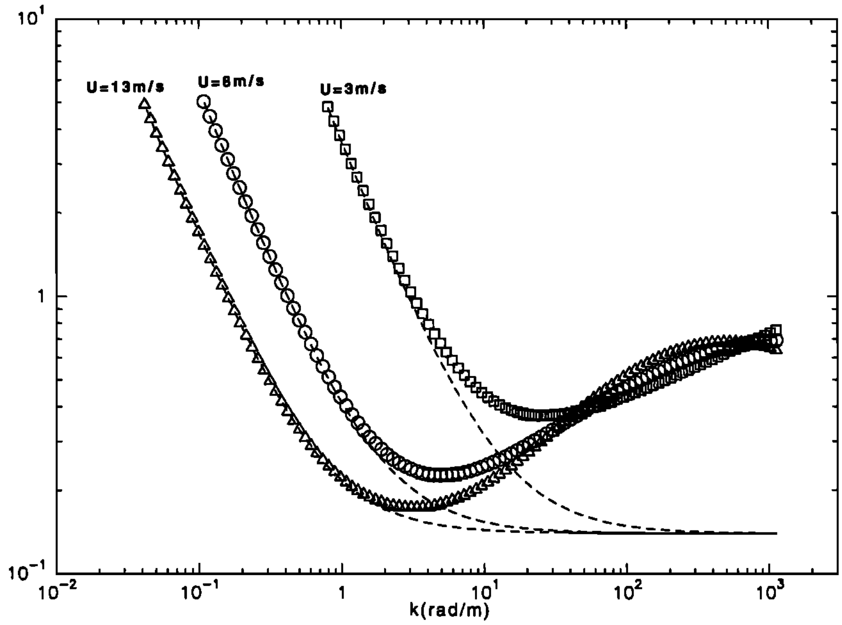

Figure 4. Modeled coefficient α of (5a) as a function of wavenumber k, for wind speed U = 3 m/s (squares), U = 8 m/s (circles), and U = 13 m/s (triangles), obtained with the six-parameter fit (equation (19)). Dashed lines represent the original expression (5b), as proposed by *Apel* [1994].

Thus (5c) provides a description of α which is quite similar to the one by *Apel* [1994] at low k, and the additional term δ becomes effective only in the spectral domain which is well constrained by our set of observations.

The most important feature appearing in Figure 4 is that the anisotropy, represented by means of coefficient α, is decreasing from the spectral peak toward high wavenumbers, then reaches a minimum, and begins to increase again as the wavenumber increases further. The minimum of α is of the order of ≈0.2 for the highest winds considered (U = 8 m/s or 13 m/s). As can be seen from Figure 1, $\alpha = 0.2$ means that the folded spreading function $D_s(k, \varphi)$ is nearly isotropic $[D_s(k, \pi/2)/D_s(k, 0) \approx 1.05]$ (even though the directional spreading function $D(k, \varphi)$ is not, since $D(k, \pi/2)/D(k, 0) \approx 0.6$). By comparison the values of α shown in Figure 4 become larger than 0.5 for k larger than 200 rad/m or so, depending upon wind speed, thus yielding a folded spreading function with a much stronger along-wind–cross-wind anisotropy, as seen from Figure 1 (for $\alpha = 0.5$, one get $D_s(k, \pi/2)/D_s(k, 0) \approx 0.6$ and $D(k, \pi/2)/D(k, 0) \approx 0.3$).

In Figure 4 the wavenumber k for which α is a minimum varies from $k \approx 20$ rad/m ($\lambda \approx 30$ cm) for U = 3 m/s to $k \approx 3$ rad/m ($\lambda \approx 2$ m) for U = 13 m/s. It is to be noted that *Banner et al.* [1989], in their analysis of the wavenumber spectra observed by a stereophotogrammetric technique, explored the wave spectrum in the wavelength range 0.2–1.6 m and reported that in this spectral domain the folded spectrum happened to be almost isotropic. This indeed corresponds to the domain where we find the low overall level of our parameter α, in full agreement with a quasi-isotropic behavior of the folded spreading function.

As can be seen in Figure 4 the additional term δ is responsible for the increase of α at high k and thus for the presence of a minimum of α at intermediate wavenumbers. The increase of α at high k is a consequence of the observational fact that radar signatures become more anisotropic as the frequency is increased. This fact was recognized by *Jones and Schroeder* [1978], who obtained a significant correlation between $\sigma^\circ_{up}/\sigma^\circ_{cr}$ and the inverse Bragg wavelength ($1/\lambda$). A scatter plot of our parameter $r = [\sigma^\circ_{al}/\sigma^\circ_{cr}]_{\mathrm{dB}}$ versus inverse Bragg wavelength is given in Figure 5, as obtained from the whole data set that we used. Note that in Figure 5 the various wind situations and both polarizations are considered and this is one of the reasons for the scatter of the data, especially at high values of $1/\lambda$. The overall rms deviation of r is 1.08 dB, and the linear regression gives an increase of r by 2.25_{dB} as $1/\lambda$ is increased by a factor of 10.

Figure 4 also allows us to examine the dependence of the term δ upon wind velocity U. Over the spectral domain probed by the radar ($9 \le k \le 1180$ rad/m) it may be seen that the anisotropy α is not substantially dependent upon wind speed. One might mention a slight increase of α with wind speed over the range $60 \le k \le 600$ rad/m. The most important dependence upon U, however, occurs at the lower wavenumbers ($k \approx 9$ rad/m) and below, in a region where the additional term δ is of little importance since the anisotropy there is dominated by the other term α_o (equation (5b)). This led us to propose a slightly less accurate but much simpler description of the anisotropy by ignoring the dependence of the correcting term δ upon velocity U (of course the anisotropy α is still dependent upon U through k_p in (5c) and (4)). Therefore instead of (19) we now take the following expression for δ:

$$\delta = \delta_2 = 10^{(p_1 X^2 + p_2 X + p_3)} \tag{21}$$

The fit to the data set converges toward the following values:

$$\begin{aligned} p_1 &= -0.177 \\ p_2 &= 1.11 \\ p_3 &= -2.00 \end{aligned} \tag{22}$$

with an rms error of 1.40 dB.

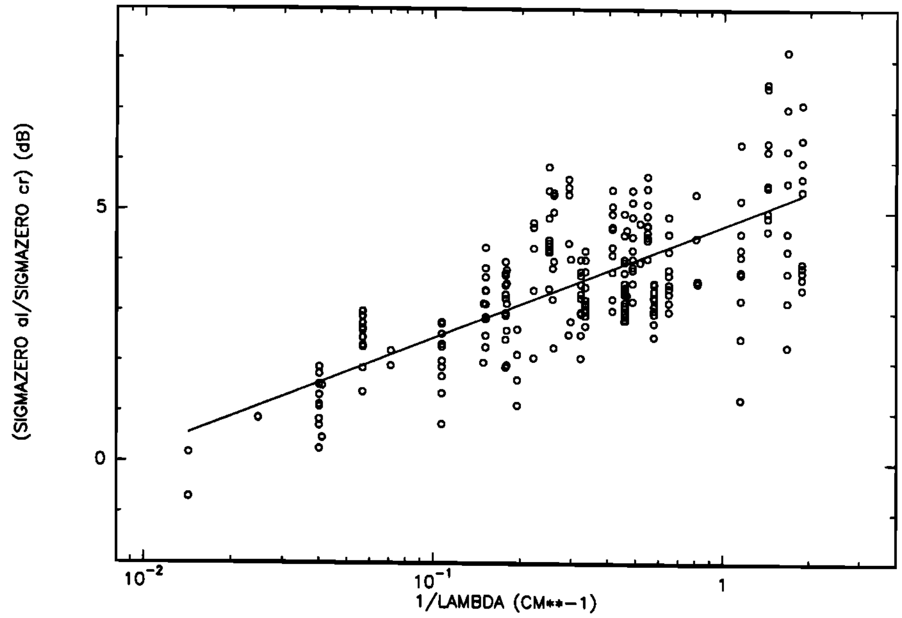

Figure 5. Scatter plot of the ratio $r = (\sigma^\circ_{al}/\sigma^\circ_{cr})$ expressed in decibels versus inverse Bragg wavelength. The solid line is the linear regression line.

The behavior of coefficient α resulting from (5a) and (5c) with (21) is displayed in Figure 6. The overall trend of α versus k is quite similar to the one of Figure 4. The location and value of the minimum of α are not significantly different from Figure 4, and (21) should therefore be sufficient for most purposes.

From (5a) and (5c) one may compute the spectral density $F(k, \varphi)$ for all directions. A more convenient way to visualize the anisotropy of the 2-D function $F(k, \varphi)$ is to examine the ratio $F(k, \pi/2)/F(k, 0)$. As discussed in section 2.1 the electromagnetic model is able to interpret the NRCS in terms of a description of the surface but is unable to determine the sense of propagation of the waves. Therefore the quantity that we are strictly able to document is rather the folded spectrum $F_s(k, \varphi) = 0.5[F(k, \varphi) + F(k, \varphi + \pi)]$ (see (8)). In Figure 7 we display the quantity $(F_{cr}/F_{al}) = F_s(k, \pi/2)/F_s(k, 0)$. In Figure 7, built from (21) and (22), the folded spectrum is clearly seen to be quasi-isotropic at intermediate scales, especially for the highest winds probed. Thus for $U = 13$ m/s the ratio (F_{cr}/F_{al}) is higher than 90% over the range $0.5 \le k \le 30$ rad/m (i.e., $0.20 \le \lambda \le 12$ m). As k increases, the ratio is reduced and amounts to no more than 35% at high wavenumbers ($k \approx 1000$ rad/m).

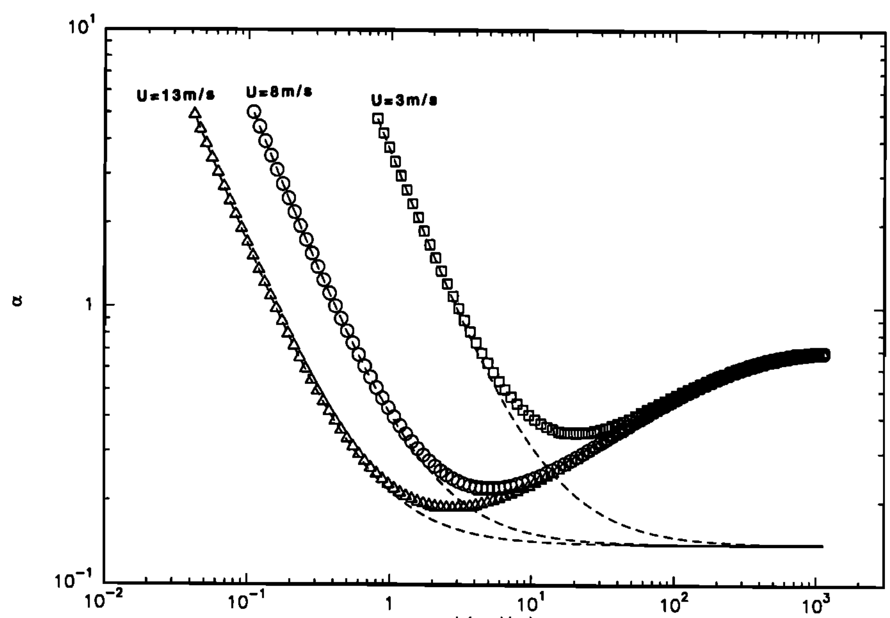

Figure 6. Same as Figure 4, but the three-parameter fit (equation (21)) is used.

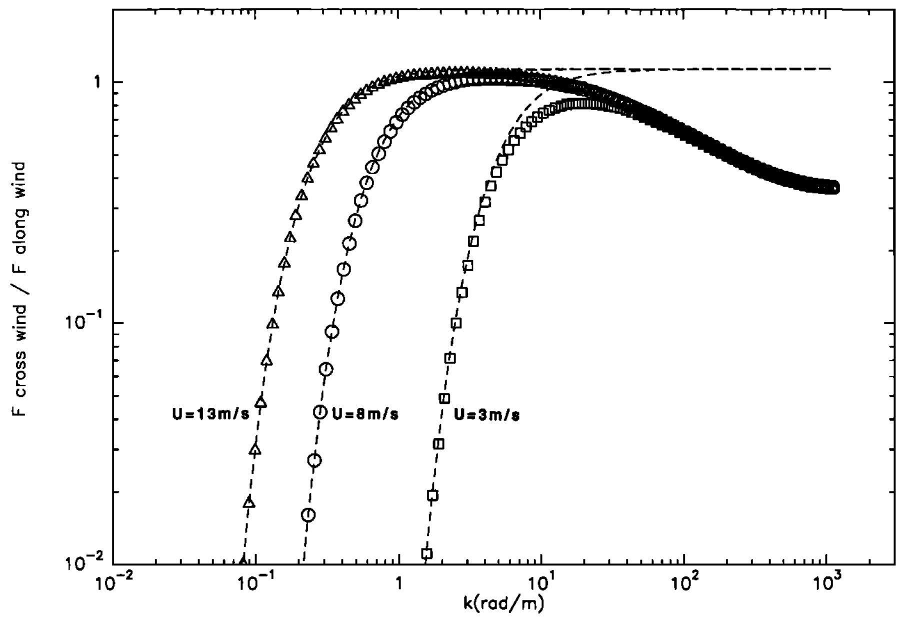

Figure 7. Ratio $F(k, \pi/2)/0.5[F(k, 0) + F(k, \pi)] = F_s(k, \pi/2)/F_s(k, 0)$ corresponding to the three-parameter fitted coefficient α displayed in Figure 6.

4.2. Spreading Function Expressed as $\text{sech}^2\ \beta\varphi$

Apel's formulation ((5a) and (5b)) for the spreading function is only an approximation to the original more complicated Donelan-Banner formulation ((2), (3a), and (3b)), which was based on a fit to observed frequency spectra. In fact, the RMS difference of $D(k, \varphi)$ between both formulations for $3 \leq U \leq 13$ m/s, over the wavenumber range not probed by our radar data set (i.e., from the peak wavenumber up to 9 rad/m) and over all directions, amounts to 10.2% of the mean of $D(k, \varphi)$. In order to conform better to Banner's original model, we have also run the model in a version where the spreading function $D(k, \varphi)$ was expressed according to (2). In that case the coefficient $\beta = \beta_o(k)$ of (3a)–(3b) is replaced by

$$\beta = \beta_o(k) + \delta \tag{23}$$

where δ is given either through (19) or through (21).

The fit with six parameters ($\delta = \delta_1$, (19)) gives the following set of parameters:

$$\begin{array}{ll} p_1 = -0.0221 & p_4 = 0.604 \\ p_2 = -0.0411 & p_5 = -0.0789 \\ p_3 = 0.0902 & p_6 = -1.66 \end{array} \tag{24}$$

with an rms error of 1.47 dB.

The fit with three parameters ($\delta = \delta_2$, (21)) gives

$$\begin{array}{l} p_1 = -0.210 \\ p_2 = 1.30 \\ p_3 = -2.27 \end{array} \tag{25}$$

with an rms error of 1.49 dB.

Both solutions for β with six or three parameters are displayed in Figure 8 and Figure 9, respectively, together with Banner's unaltered coefficient β_o. Although the formulation is different, β exhibits a behavior versus k which is similar to the one of previous coefficient α, with a minimum occurring in the range $5 \leq k \leq 20$ rad/m (i.e., $0.30 \leq \lambda \leq 1.3$ m), depending upon the wind velocity. Figure 10 displays the quantity (F_{cr}/F_{al}) as defined in section 4.1, for the three-parameter fit. One sees in Figure 10 that over a large wavenumber domain the folded wave spectrum is virtually isotropic ($F_{cr}/F_{al} \approx 1$), especially for high winds. At high frequencies, Figure 10 is indeed very similar to Figure 7, as expected since the same data set is used. The main difference occurs at low frequencies and is due to the difference between the Donelan-Banner and Apel formulations.

5. Conclusion and Discussion

By using multifrequency microwave observations of the normalized radar cross section $\sigma°$ from P band (frequency = 0.43 GHz) up to Ka band (frequency = 34.43 GHz), together with optical observations of the sea surface slope variance, we have constrained a model of the wave spectral directional spreading function $D(k, \varphi)$ for $3 \leq U \leq 13$ m/s. Two formulations were given, one providing a high-wavenumber extrapolation to *Apel*'s [1994] formulation and the other to *Donelan et al.*'s [1985] and *Banner*'s [1990] formulation, through the introduction of a correcting term δ in (5c) or (23). The term δ is a function of both k and U, which varies strongly with k and slightly with U. Expression (21), involving only k, with three adjusted parameters given by (22) or (25) according to the formulation used, provides a formulation for δ which should be sufficient for most purposes. We suggest that *Apel*'s [1994] or *Banner*'s [1990] expressions for $D(k, \varphi)$ should be corrected accordingly, to account for the behavior of $D(k, \varphi)$ at high wavenumbers. If one wishes a more accurate formulation where the dependence upon U is accounted for, one may then use the six-parameter expression (19) for δ. Such formulation for $D(k, \varphi)$ is given from near the spectral peak up to $k \approx 1180$ rad/m.

According to this spreading function, there is a spectral region in the short gravity range where the folded spectrum is nearly isotropic, in accordance with *Banner et al.*'s [1989] stereophotogrammetric observations. However, a noticeable fea-

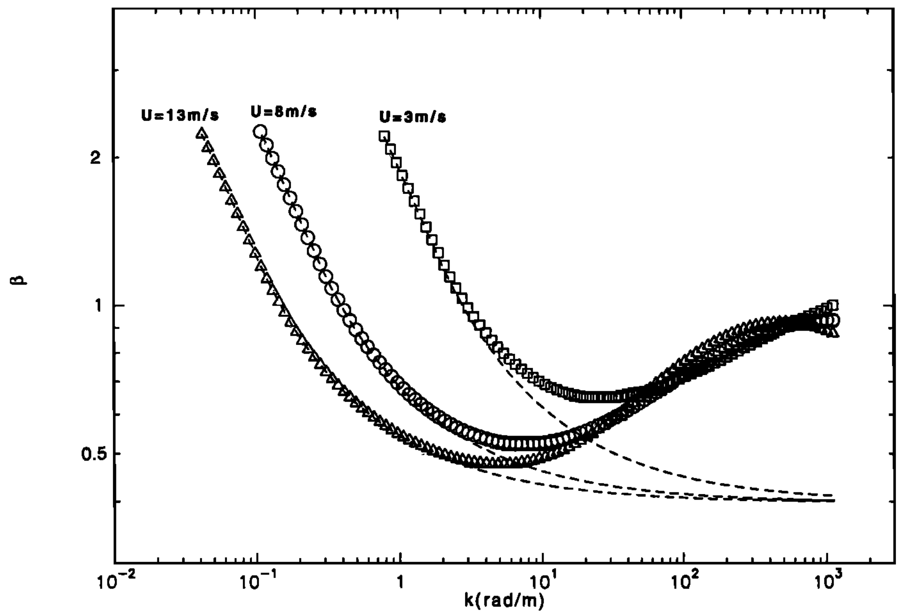

Figure 8. Modeled coefficient β of (2), as a function of wavenumber k for U = 3 m/s, U = 8 m/s, and U = 13 m/s, obtained with the six-parameter fit. Dashed lines represent original formulation (3a)–(3b), as proposed by *Banner* [1990].

ture of our model is that unlike Apel's model, it gives an increase of the anisotropy of the spreading function at higher wavenumbers, in such a way that the ratio between the cross-wind and along-wind spectral densities of the folded spectrum reaches only 35% at high wavenumbers (k ≈ 1000 rad/m).

Such an increase of anisotropy at high k is in accordance with *Donelan and Pierson*'s [1987] semiphysical model. The reason for this behavior in Donelan and Pierson's model was that the wind-induced growth rate of the sea waves that they use becomes more sensitive to the direction at high k. However, our more precise six-parameter fit, illustrated by Figures 4 and 8, shows that over the range $50 \leq k \leq 500$ rad/m, the anisotropy tends to slightly increase with increasing wind. Over the same range, Donelan and Pierson's model would instead predict an anisotropy slightly decreasing with wind speed. Our results, both in terms of the wavenumber dependence and wind dependence of the anisotropy, conform to the conclusions drawn by *Fung and Lee* [1982] from *Ku* band data and by *Caudal and Le Proud'hom* [1994] from *C* band data. However, those previous results involved only limited radar frequency bands and were therefore unable to document a wide range of wavenumbers.

Expressing the azimuthal behavior of the spectrum in terms of a simple spreading function $D(k, \varphi)$ such as the ones given

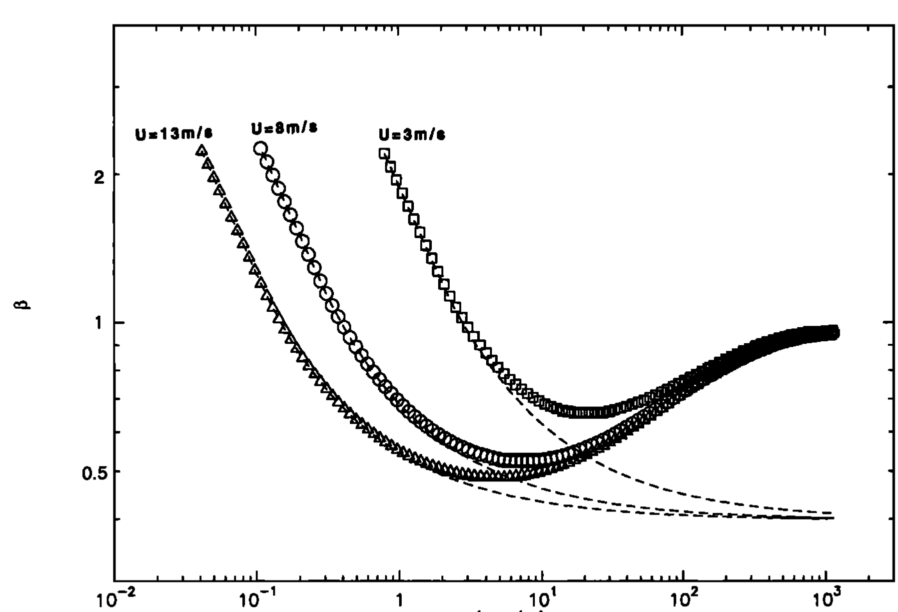

Figure 9. Same as Figure 8, but the three-parameter fit is used.

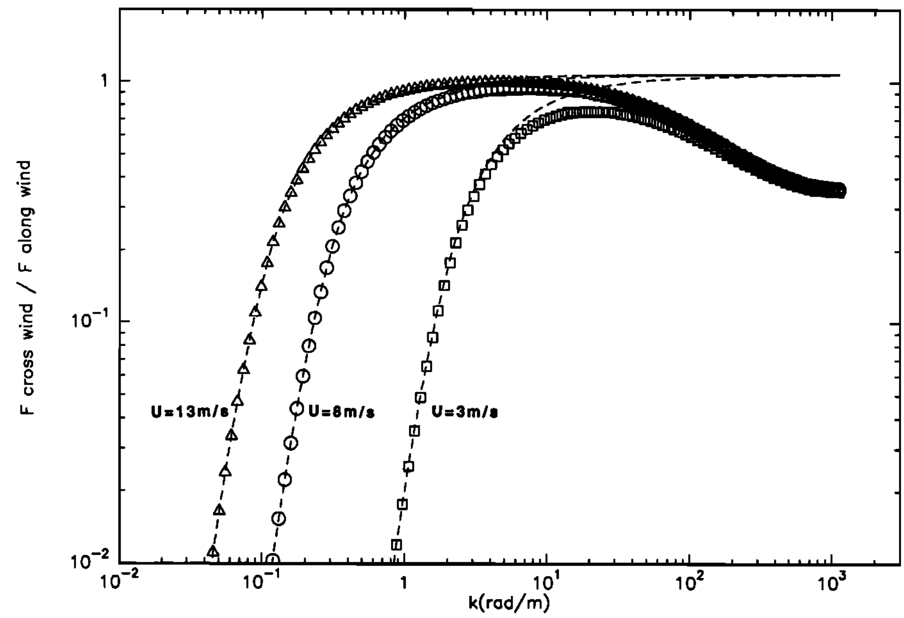

Figure 10. Ratio $F(k, \pi/2)/0.5[F(k, 0) + F(k, \pi)]$ corresponding to the three-parameter fitted coefficient β displayed in Figure 9.

by (2) or (5a) is of course an idealization. Recently, *Banner and Young* [1994] performed sea wave modeling studies, in which they relaxed the assumption of a constrained spectral tail usually done in wave modeling. They obtained a transition of the directional spreading from unimodal mode near the spectral peak to bimodal mode with increasing wavenumber. Those results seem to be corroborated by the field measurements performed by *Young et al.* [1995] who observed the sea wave directional spectrum up to 4 times the peak frequency f_p and reported the bimodal structure becoming apparent at wave frequencies above $2f_p$. It would be interesting to explore whether such bimodal features have a signature at the short scales sampled by the radars. However, a bimodal directional spectrum would usually give a folded spectrum with four maxima, and even with the more sophisticated NRCS models presently available, the azimuthal description of σ^0 is too coarse to distinguish such refined features.

Ideally, when combining multifrequency radar observations as is done in this paper, one would like to obtain detailed information on the complete high-wavenumber spectrum. This involves not only the azimuthal behavior but also the absolute spectral level in the wind direction and its dependence upon both wavenumber and wind speed. We intended to focus this paper on the azimuthal signature alone because some of the data sets used here do not involve absolute measurements of σ^0 but only relative variations of σ^0 with wind direction or amplitude. Also, the azimuthal behavior at high wavenumbers seems to be the most poorly documented feature in the existing wave spectral models. Work aiming at constraining the complete high-wavenumber spectrum by means of multifrequency radar measurements is underway.

Finally, one should note that our description of the sea surface only involves its 2-D spectrum, assuming independence of the various spectral components. Some phase relations among the spectral components are, however, expected to occur, reflecting hydrodynamic modulations and localized features (wedges, spilling breakers, hydraulic jumps) [*Donelan and Pierson*, 1987]. As discussed by *Caudal and Le Proud'hom* [1994], the high-order Fourier terms which are needed to describe a localized feature such as a sharp wedge are formally included in the calculation, but the simplification made concerns the phases of those Fourier terms, which we assume here to be distributed randomly. Within this limitation, which is inherent to the electromagnetic modeling and surface description used, such remote sensing techniques seem to provide the most efficient way to get a realistic extrapolation of the spreading function to high wavenumbers.

Appendix A: *Apel's* [1994] Model for *F(k, 0)*

The section through the wave number spectrum in the wind direction $F(k, 0)$ is given by *Apel* [1994] as follows:

$$F(k, 0) = 0.00195 L_o J_p H_t k^{-4} \quad \text{(A1)}$$

where

$$L_o = \exp[-(k_p/k)^2] \quad \text{(A2)}$$

Here k_p is the spectral peak which, for full development, is given by (4).

J_p is expressed as follows:

$$J_p(k) = 1.7^{\gamma_o(k)} \quad \text{(A3)}$$

where

$$\gamma_o(k) = \exp[-(k^{1/2} - k_p^{1/2})^2/0.32k_p] \quad \text{(A4)}$$

Finally, H_t is given as

$$H_t = [R_{ro} + SR_{\text{res}}] \exp(-k^2/k_{\text{dis}}^2) \quad \text{(A5)}$$

with

$$R_{ro} = \frac{1}{1 + (k/k_{ro})^2} \quad \text{(A6)}$$

$$R_{res} = 0.8\ k\ \mathrm{sech}[(k - k_{res})/k_w] \tag{A7}$$

$$S = \exp\{[-4.95 + 3.45(1 - e^{-U/U_\eta})]\ln 10\} \tag{A8}$$

The constants introduced here are $k_{dis} = 6283$ rad/m, $k_{ro} = 100$ rad/m, $k_{res} = 400$ rad/m, $k_w = 450$ rad/m, and $U_\eta = 4.7$ m/s.

Appendix B: Electromagnetic Model

We compute the normalized radar cross section σ° of the sea surface through the standard two-scale theory [*Valenzuela*, 1978; *Ulaby et al.*, 1982]. This yields [*Donelan and Pierson*, 1987]

$$\sigma_{HH}{}^\circ(\theta_i) = 16\pi k_o{}^4 \cos^4 \theta_i \left| \left(\frac{\mu \cos \delta}{\mu_i}\right)^2 g_{HH}(\theta_i) + \left(\frac{\sin \delta}{\mu_i}\right)^2 g_{VV}(\theta_i) \right|^2 F_{s1}(2k_o\mu,\ 2k_o\gamma \sin \delta) \tag{B1}$$

$$\sigma_{VV}{}^\circ(\theta_i) = 16\pi k_o{}^4 \cos^4 \theta_i \left| \left(\frac{\mu \cos \delta}{\mu_i}\right)^2 g_{VV}(\theta_i) + \left(\frac{\sin \delta}{\mu_i}\right)^2 g_{HH}(\theta_i) \right|^2 F_{s1}(2k_o\mu,\ 2k_o\gamma \sin \delta) \tag{B2}$$

$$\sigma_{pp}{}^{osea}(\theta) = \int_{-\infty}^{\infty} d(\tan \Psi) \int_{-\infty}^{\infty} d(\tan \delta) \sigma_{pp}{}^\circ(\theta_i) P(\tan \Psi, \tan \delta) \tag{B3}$$

In those equations, k_o is the wavenumber of the electromagnetic wave, θ is the radar incidence angle, and Ψ and δ are the angular deviations of the normal to the surface caused by the tilting waves in and perpendicular to the plane of incidence, respectively. The resulting local angle of incidence is $\theta_i = \cos^{-1}[\cos(\theta + \Psi)\cos\delta]$. Also, $\mu_i = \sin\theta_i$, $\mu = \sin(\theta + \Psi)$, and $\gamma = \cos(\theta + \Psi)$. Subscript pp in (B3) stands for either HH (horizontal polarization) or VV (vertical polarization), and g_{HH} and g_{VV} are given by

$$g_{HH}(\theta) = \frac{(\varepsilon_r - 1)}{[\cos\theta + (\varepsilon_r - \sin^2\theta)^{1/2}]^2} \tag{B4}$$

$$g_{VV}(\theta) = \frac{(\varepsilon_r - 1)[\varepsilon_r(1 + \sin^2\theta) - \sin^2\theta]}{[\varepsilon_r \cos\theta + (\varepsilon_r - \sin^2\theta)^{1/2}]^2} \tag{B5}$$

In (B4) and (B5), ε_r is the relative (complex) dielectric constant of the water. Empirical expressions of ε_r for saline water as a function of frequency, temperature, and salinity were reviewed by *Ulaby et al.* [1986] according to the work by *Stogryn* [1971] and *Klein and Swift* [1977]. Those expressions are used in this paper, with a temperature of 10°C and a salinity of 32.5 parts per thousand.

The folded polar spectrum $F_s(k, \varphi)$ (see section 2.1.2) and the folded Cartesian spectrum $F_{s1}(k_x, k_y)$ are normalized ac cording to

$$\langle \zeta^2 \rangle = \int_{-\infty}^{\infty}\int_{-\infty}^{\infty} F_{s1}(k_x, k_y)\, dk_x dk_y = \int_{-\pi}^{\pi}\int_{o}^{\infty} F_s(k, \varphi)\, k dk d\varphi \tag{B6}$$

where $\langle \zeta^2 \rangle$ is the variance of the surface elevation.

In (B3), $P(\tan\Psi, \tan\delta)$ is the joint probability density function for the slopes of the tilting waves, adjusted to account for geometrical corrections (see *Donelan and Pierson*'s [1987] equation (31) and discussion therewith). We assume a Gaussian pdf, which may then be computed provided that the along-wind and cross-wind slope variances are known. The slope variance in either the along-wind or the cross-wind direction can be determined from the full wavenumber spectrum by a mere 2-D integration of the slope spectrum $k_x{}^2F_{s1}(k_x, k_y)$ or $k_y{}^2F_{s1}(k_x, k_y)$, respectively (where the k_x direction is supposed here to be directed along the wind). Such an integration has to be performed from $k = 0$ up to the high-wavenumber cutoff of the tilting waves k_Γ. A difficulty in applying a two-scale model is choosing an appropriate value for k_Γ, because the results are weakly dependent upon the choice of k_Γ. Following *Donelan and Pierson* [1987], we take $k_\Gamma = k_B/\Gamma$, where $\Gamma = 40$ and k_B is the Bragg wavenumber ($k_B = 2k_o \sin\theta$).

Finally, we add the specular component which reads [*Valenzuela*, 1978; *Donelan and Pierson*, 1987]

$$\sigma^\circ{}_s = \frac{|R(0)|^2 \sec^4\theta}{2[S_x][S_y]} \exp\left(-\frac{\tan^2\theta}{2S_L{}^2}\right) \tag{B7}$$

where $[S_x]$ and $[S_y]$ are the along-wind and cross-wind slope standard deviations of waves with wavenumbers k_o/Γ and smaller and $S_L{}^2$ is the slope variance in the plane of incidence, given by

$$S_L{}^2 = \frac{S_x{}^2 S_y{}^2}{S_y{}^2\cos^2\varphi + S_x{}^2\sin^2\varphi} \tag{B8}$$

where φ is the azimuthal angle between the radar beam direction and the wind direction.

In (B7) the reflection coefficient at normal incidence $|R(0)|$ is given as

$$|R(0)| = |0.65(\varepsilon_r - 1)/(\varepsilon_r{}^{1/2} + 1)^2| \tag{B9}$$

References

Apel, J. R., An improved model of the ocean surface wave vector spectrum and its effects on radar backscatter, *J. Geophys. Res.*, *99*(C8), 16,269–16,291, 1994.

Banner, M. L., Equilibrium spectra of wind waves, *J. Phys. Oceanogr.*, *20*, 966–984, 1990.

Banner, M. L., and I. R. Young, Modeling spectral dissipation in the evolution of wind waves, I, Assessment of existing model performance, *J. Phys. Oceanogr.*, *24*, 1550–1571, 1994.

Banner, M. L., I. S. F. Jones, and J. C. Trinder, Wavenumber spectra of short gravity waves, *J. Fluid Mech.*, *198*, 321–344, 1989.

Bentamy, A., Y. Quilfen, P. Queffeulou, and A. Cavanie, Calibration of the ERS-1 scatterometer C-band model, *Tech. Rep. DRO/OS-94-01*, Inst. Fr. de Rech. pour l'Exploit. de la Mer, Brest, France, 1994.

Caudal, G., and E. Le Proud'hom, Anisotropy of the sea spectrum at 3-30cm wavelengths, inferred from C-band radar sea echo model, *Int. J. Remote Sens.*, *15*(3), 657–667, 1994.

Cox, C., and W. Munk, Measurement of the roughness of the sea surface from photographs of the sun's glitter, *J. Opt. Soc. Am.*, *44*(11), 838–850, 1954.

Daley, J., An empirical sea clutter model, *NRL Memo. Rep. 2668*, 1973.

Donelan, M. A., and W. J. Pierson Jr., Radar scattering and equilibrium ranges in wind-generated waves with application to scatterometry, *J. Geophys. Res.*, *92*(C5), 4971–5029, 1987.
Donelan, M. A., J. Hamilton, and W. H. Hui, Directional spectra of wind-generated waves, *Philos. Trans. R. Soc. London A*, *315*, 509–562, 1985.
Durden, S. L., and J. F. Vesecky, A physical radar cross-section model for a wind-driven sea with swell, *IEEE J. Oceanic Eng.*, *OE-10*(4), 445–451, 1985.
Eymard, et al., Experimental study of ocean-atmosphere exchanges, paper presented at the Second International Conference on air-sea interaction and on meteorology and oceanography of the coastal zone, Am. Meteorol. Soc., Lisbon, Portugal, 1994.
Fung, A. K., and K. K. Lee, A semi-empirical sea-spectrum model for scattering coefficient estimation, *IEEE J. Oceanic Eng.*, *OE-7*(4), 166–176, 1982.
Hasselmann, D. E., M. Dunckel, and J. A. Ewing, Directional wave spectra observed during JONSWAP 1973, *J. Phys. Oceanogr.*, *5*, 1264–1280, 1980.
Hauser, D., G. Caudal, G.-J. Rijckenberg, D. Vidal-Madjar, G. Laurent, and P. Lancelin, RESSAC: A new airborne FM/CW radar ocean wave spectrometer, *IEEE Trans. Geosci. Remote Sens.*, *30*, 981–995, 1992.
Jackson, D. D., Interpretation of inaccurate, insufficient and inconsistent data, *Geophys. J. R. Astron. Soc.*, *28*, 97–109, 1972.
Jahne, B., and K. S. Riemer, Two-dimensional wave number spectra of small-scale water surface waves, *J. Geophys. Res.*, *95*(C7), 11,531–11,546, 1990.
Jones, W. L., and L. C. Schroeder, Radar backscatter from the ocean: Dependence on surface friction velocity, *Boundary Layer Meteorol.*, *13*, 133–149, 1978.
Klein, L. A., and C. T. Swift, An improved model for the dielectric constant of sea water at microwave frequencies, *IEEE Trans. Antennas Propag.*, *AP-25*, 104–111, 1977.
Masuko, H., K. Okamoto, M. Shimada, and S. Niwa, Measurement of microwave backscattering signatures of the ocean surface using X band and K_a band airborne scatterometers, *J. Geophys. Res.*, *91*(C11), 13,065–13,083, 1986.
Snoeij, P., P. J. F. Swart, and C. M. H. Unal, Study on the response of the radar echo from the ocean surface to the surface wind vector at frequencies between 1 and 18 GHz, *Final Rep. Eur. Space Agency, Contract 8722/89/F/FL(SC)*, Eur. Space Agency, Neuilly, France, 1992.
Stogryn, A., Equations for calculating the dielectric constant of saline water, *IEEE Trans. Microwave Theory Tech.*, *MIT-19*, 733–736, 1971.
Ulaby, F. T., R. K. Moore, and A. K. Fung, *Microwave Remote Sensing: Active and Passive*, vol. II, *Radar Remote Sensing and Surface Scattering and Emission Theory*, pp. 922–1033, Artech House, Norwood, Mass., 1982.
Ulaby, F. T., R. K. Moore, and A. K. Fung, *Microwave Remote Sensing: Active and Passive*, vol. III, *From Theory to Applications*, pp. 2017–2119, Artech House, Norwood, Mass., 1986.
Unal, C. M. H., P. Snoeij, and P. J. F. Swart, The polarization-dependent relation between radar backscatter from the ocean surface and surface wind vector at frequencies between 1 and 18 GHz, *IEEE Trans. Geosci. Remote Sens.*, *29*(4), 621–626, 1991.
Valenzuela, G. R., Theories for the interaction of electromagnetic and oceanic waves—A review, *Boundary Layer Meteorol.*, *13*, 61–85, 1978.
Young, I. R., L. A. Verhagen, and M. L. Banner, A note on the bimodal directional spreading of fetch-limited wind waves, *J. Geophys. Res.*, *100*(C1), 773–778, 1995.

G. Caudal and D. Hauser, Centre d'Étude des Environnements Terrestre et Planétaires, 10-12 Avenue de l'Europe, 78140 Vélizy, France. (e-mail: gerard.caudal@cetp.ipsl.fr;daniele.hauser@cetp.ipsl.fr)

(Received July 12, 1995; revised March 18, 1996; accepted March 20, 1996.)